Received Power Characterization of Terrestrial Cellular Signals on High Altitude Aircraft

Zaher M. Kassas
Department of Mechanical and Aerospace Engineering
University of California, Irvine
Irvine, CA 92697
zkassas@ieee.org

Ali A. Abdallah
Department of Electrical Engineering and Computer Science
University of California, Irvine
Irvine, CA 92697
abdalla2@uci.edu

Joe Khalife
Department of Mechanical and Aerospace Engineering
University of California, Irvine
Irvine, CA 92697
khalifej@uci.edu

Chiawei Lee, Juan Jurado, Steven Wachtel, Jacob duede, Zachary Hoeffner, Thomas Hulsey, Rachel Quirarte, and RunXuan Tay
U.S. Air Force
Edwards, CA 93524

***Abstract*— The received power of terrestrial cellular 3G code division multiple access (CDMA) and 4G long-term evolution (LTE) signals on a high altitude aircraft is experimentally characterized. The conducted experiments were performed on a Beechcraft C-12 Huron, a fixed-wing U.S. Air Force aircraft. Two types of flight patterns were performed: (i) teardrop-like patterns to characterize the carrier-to-noise ratio (C/N_0) versus altitude and (ii) grid-like patterns to characterize C/N_0 versus the horizontal distance between the aircraft and cellular towers. Flight campaigns in two regions were conducted: (i) a rural region in Edwards, California, USA, and (ii) an urban region in Riverside, California, USA. It was observed that cellular signals are surprisingly powerful at both (i) high altitudes, exhibiting C/N_0 of 25–55 dB-Hz at altitudes of 2,000–23,000 ft above ground level (AGL) and (ii) faraway horizontal distances, exhibiting C/N_0 of about 30 dB-Hz for towers as far as 50 km, while flying at about 16,000 ft AGL. In addition, two propagation models were evaluated to describe the behavior of the measured C/N_0: (i) free-space path loss model and (ii) two-ray model. It was observed that the two-ray model fits the measured C/N_0 sufficiently well, for towers more than 10 km away, while flying at an altitude of 16,000 ft AGL. For towers closer than 10 km, the antenna radiation pattern should be incorporated into the two-ray model to improve model fitting.**

TABLE OF CONTENTS

1. INTRODUCTION

Global navigation satellite systems (GNSS) are heavily relied upon in today's aviation communications, navigation, and surveillance (CNS) systems as well as air traffic management [1]. The upsurge in GNSS radio frequency interference (RFI) is jeopardizing safe and efficient aviation operations [2, 3]. RFI sources include repeaters and pseudolites [4, 5], GNSS jammers [6, 7], and systems transmitting outside the GNSS frequency bands [8, 9]. There were 4,364 GNSS outages reported by pilots in 2018, which represents more than a 2,000% increase over the previous year [10]. What is alarming is that RFI is affecting civil aviation at distances of up to 300 km from conflict zones (where GNSS jammers tend to be prevent) and that the majority of RFI (about 81%) affects en-route flights. In 2019, the International Civil Aviation Organization (ICAO) issued a Working Paper titled "An Urgent Need to Address Harmful Interferences to GNSS," where it concluded that harmful RFI to GNSS would prevent the full continuation of safety and efficiency benefits of GNSS-based services. Moreover, there was a call for supporting multi-disciplinary development of alternative positioning, navigation, and timing (PNT) strategy and solutions to complement the use of GNSS in aviation [11].

Cellular signals have shown tremendous promise as an alternative PNT source [12–23]. This is due to their inherently desirable attributes [24]: (i) they are ubiquitous, (ii) they are transmitted in a wide range of frequencies and in many directions which makes them spectrally and geometrically diverse, (iii) they possess a high received carrier-to-noise (C/N_0) ratio (tens of dBs higher than GNSS), and (iv) they are readily available for free as their infrastructure is well established and the signals are broadcasted to billions of users worldwide. Recent results have shown the ability of cellular signals to yield meter-level-accurate navigation on ground vehicles [25–29] in urban environments and submeter-level-accurate navigation on UAVs [30, 31]. Moreover, the robustness and availability of cellular signals have been demonstrated in a GPS-jammed environment [32].

Assessing cellular signals for aerial vehicles has been the subject of several studies recently [33–37]. It was concluded that commercial cellular networks are capable of providing connectivity to aerial vehicles at low altitudes [38, 39]. However, the majority of existing studies considered low altitude aerial vehicles traveling at low speeds and focused on evaluating cellular signals for communication purposes with little attention to evaluating them for PNT [40].

A joint effort between the Autonomous Systems Perception, Intelligence, and Navigation (ASPIN) Laboratory and Edwards Air Force Base, California, USA led to a weeklong flights in March 2020 in a mission called "SNIFFER: Signals of opportunity for Navigation In Frequency-Forbidden EnviRonments." The flights took place on a Beechcraft C-12 Huron, a fixed-wing U.S. Air Force aircraft, to study the efficacy of terrestrial cellular signals for aircraft navigation. This paper presents findings from these flights to characterize

978-1-6654-3760-8/22/$31.00 ©2022 IEEE

C/N_0 of terrestrial cellular 3G code division multiple access (CDMA) and 4G long-term evolution (LTE) signals. The C/N_0 provides a measure of the precision of the navigation observables (pseudorange and carrier phase) [41], which are used to calculate the PNT solution [42, 43]. Two types of flight patterns were performed: (i) teardrop-like patterns to characterize the carrier-to-noise ratio (C/N_0) versus altitude and (ii) grid-like patterns to characterize C/N_0 versus the horizontal distance between the aircraft and cellular towers. Flight campaigns in two regions were conducted: (i) a rural region in Edwards, California, USA, and (ii) an urban region in Riverside, California, USA. It was observed that cellular signals are surprisingly powerful at both (i) high altitudes, exhibiting C/N_0 of 25–55 dB-Hz at altitudes of 2,000–23,000 ft above ground level (AGL) and (ii) faraway horizontal distances, exhibiting C/N_0 of about 30 dB-Hz for towers as far as 50 km, while flying at about 16,000 ft AGL. In addition, two propagation models were evaluated to describe the behavior of the measured C/N_0: (i) free-space path loss model and (ii) two-ray model. It was observed that the two-ray model fits the measured C/N_0 sufficiently well, for towers more than 10 km away, while flying at an altitude of 16,000 ft AGL. For towers closer than 10 km, the antenna radiation pattern should be incorporated into the two-ray model to improve model fitting to the measured C/N_0.

The remainder of the paper is organized as follows. Section 2 overviews (i) hardware and software setup, (ii) flight maneuvers, and (iii) flight regions. Section 3 characterizes the measured C/N_0 of 3G and 4G cellular signals as a function of altitude and horizontal distance to the towers in the both regions. It also evaluates the free-space path loss model and the two-ray model. Section 4 gives concluding remarks.

2. High-Altitude Aircraft Navigation with Terrestrial Cellular Signals

This section presents the hardware and software setup with which the aircraft was equipped and flight maneuvers and regions.

Hardware and Software Setup

The C-12 aircraft was equipped with a universal software radio peripheral (USRP) with consumer-grade cellular antennas to sample three cellular bands and store the samples on a desktop computer for off-line processing. The stored samples were post-processed with the 3G and 4G cellular modules of ASPIN Laboratory's SDR, called MATRIX: Multichannel Adaptive TRansceiver Information eXtractor [32]. The SDR produces navigation observables: Doppler frequency, carrier phase, and pseudorange, along with the corresponding C/N_0. The hardware setup is shown in Figure 1.

Flight Maneuvers

Two types of maneuvers were performed in each region. The first is a teardrop-like pattern while climbing/descending. The pattern has a focal point that is aligned with a geographic point of interest. The measurements used to characterize C/N_0 and multipath were taken exactly above the geographic point of interest to maintain the horizontal distance between the aircraft and the cellular base stations. The second type of maneuver is a grid-like pattern with many turns and straight segments. Such patterns were used as a stress test on ASPIN Laboratory's SDRs to assess the performance of signal acquisition, tracking loops, and navigation solution. The two types of maneuvers are shown in Figure 2.

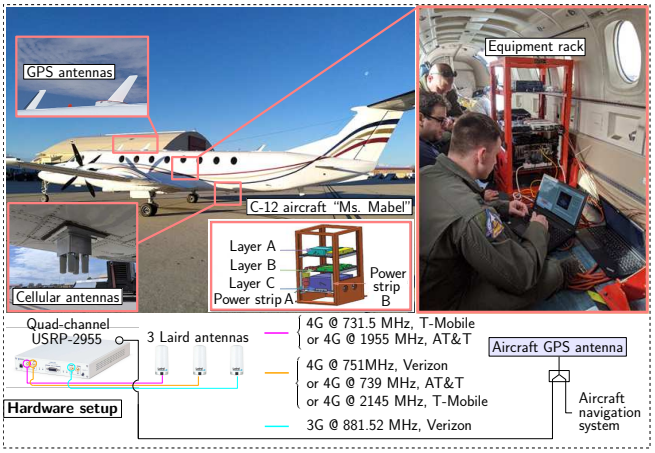

Figure 1. Hardware setup with which the C-12 aircraft was equipped.

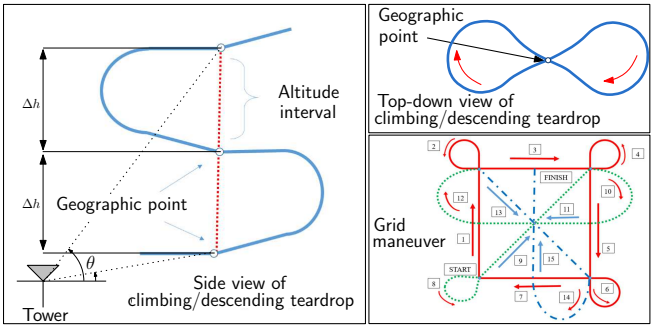

Figure 2. Maneuvers performed by the C-12 aircraft. The altitude step and elevation angle are denoted by Δh and θ, respectively.

Flight Regions

Figure 3 shows the regions in which the experiments were performed: (i) Region A, a rural region in Edwards, California, USA and (ii) Region C, an urban region in Riverside, California, USA.

3. Received C/N_0 Characterization

This section characterizes the C/N_0 of received cellular signals in regions A and C. Different channel models are evaluated to find the best model that represents the C/N_0 behavior. The precision of navigation observables (pseudorange and carrier phase) is a function of C/N_0, which ultimately determines the precision of the navigation solution. As its name suggests, the pseudorange is not quite the range between the transmitter and the receiver, but the sum of the range and the bias due to the difference between the transmitter and receiver's clocks. Essentially, the pseudorange measurement is constructed by measuring the time-of-arrival (TOA) of the signal. The TOA is obtained by correlating the received cellular signals with known synchronization sequences [24]. The C/N_0 can be calculated according to [41]

$$C/N_0 = \frac{C}{N_0} = \frac{C}{\sigma^2_{\text{noise}} T},$$

where C is the carrier power in Watts (W), N_0 is the noise power spectral density in W/Hz, which can b expressed as $N_0 = \sigma^2_{\text{noise}} T$, where $\sigma^2{}_{\text{noise}}$ is the discretized noise variance

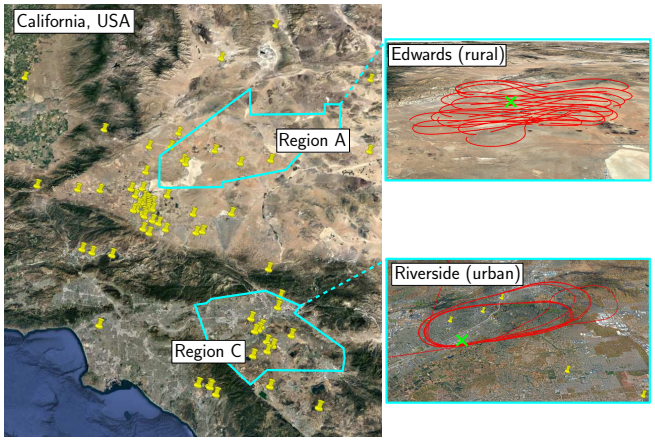

Figure 3. Regions A and C in which the flight campaigns took place. The yellow pins in the left figure represent 3G and 4G cellular towers that were mapped and analyzed in this study. The right figures show the aircraft trajectory in both regions (shown in red). Geographic points of interest in each region, shown in green crosses, were chosen according to the designed trajectories.

and T is the accumulation period, or the period over which correlation is performed. Typically, the C/N_0 should be above 35 dB-Hz for reliable acquisition, and above 25 dB-Hz to maintain track [41]. High sensitivity receivers can acquire and track at lower values of C/N_0 [44–46].

Free-Space Path Loss Model

The free-space path loss (FSPL) model is a simple, yet informative for aerial vehicles' wireless channels. The FSPL accounts only for the propagation loss between two isotropic radiators in free space and can be expressed as [47]

$$\frac{C}{N_0}(h) = \frac{C}{N_0}(R_0) - 10\alpha \log_{10} \sqrt{D} + w, \qquad (1)$$

where R_0 is the initial range; D is the line-of-sight given by $D = d^2 + h^2$, where d and h are the horizontal and vertical distances to the tower, respectively; α is the pathloss exponent; and w is a zero-mean random variable. Figure 4 depicts the variables involved in the FSPL model.

The measured C/N_0 as a function of altitudes for Region A and both signal types (3G CDMA and 4G LTE) are shown in Figures 5 and 6. Also shown are the FSPL model fit, where the pathloss exponent was assumed to be $\alpha = 2$ (free space). The aircraft-mounted SDR was able to maintain tracking of all acquired cellular signals up to the maximum altitude it reached, namely 23,000 ft AGL.

The C/N_0 for six 3G and 4G base stations in Region C are plotted as a function of the horizontal distance in Figure 7. It is worth noting that the aircraft was flying at an altitude of a little above 16,000 ft AGL. At such an altitude, the elevation angles are very high. Since cellular base station antennas are tilted downwards and are directional in the elevation direction, the loss due to the directive radiation pattern of cellular base station antennas dominate the pathloss. This explains why some of the C/N_0s in Figure 7 have an increasing trend, especially at shorter horizontal distances where the change in elevation angle is more significant. The big hole between 22 to 38 km in Figure 7 is purely due to the fact that some cellular towers happened to be located either too close or too far with respect to the trajectory traversed by the aircraft. In other words, none of the lines get disconnected in this gap; instead, the C/N_0 of the two base stations in the region below the 22 km horizontal distance are different from the four base stations in the region right to the 38 km horizontal distance. The aircraft-mounted SDR was able to maintain tracking of cellular towers as far as 50 km away.

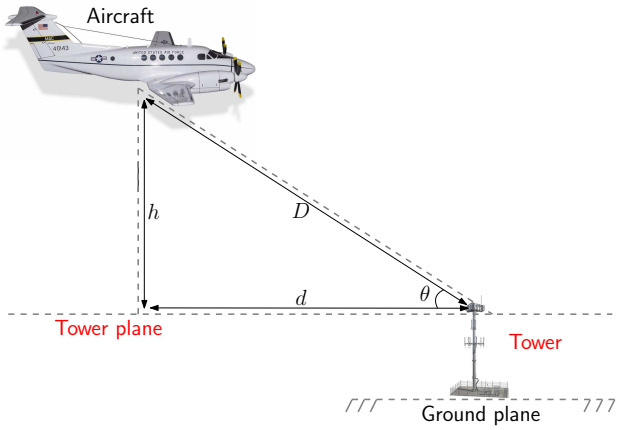

Figure 4. The free path loss model diagram.

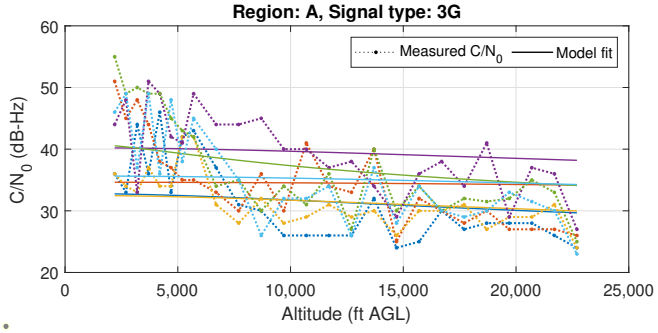

Figure 5. The C/N_0 of 7 3G towers as a function of altitude in Region A. The model fit is obtained by fitting the measured data to (1) for $\alpha = 2$.

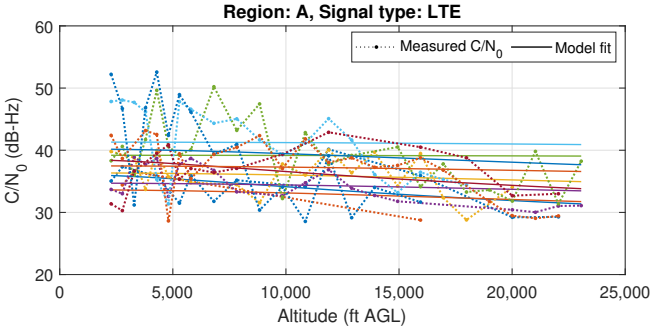

Figure 6. The C/N_0 of 14 4G towers as a function of altitude in Region A. The model fit is obtained by fitting the measured data to (1) for α=2.

Two-Ray Model

Next, a more sophisticated model is evaluated, namely the two-ray model. The two-ray model can be expressed as [47]

$$\frac{C}{N_0}(D) = \frac{C}{N_0}(D_0) - 20 \log_{10} \left[r_p \left| \frac{1}{D} + \Gamma(\psi) \frac{e^{-j\Delta\phi}}{D + \Delta D} \right| \right],$$

where

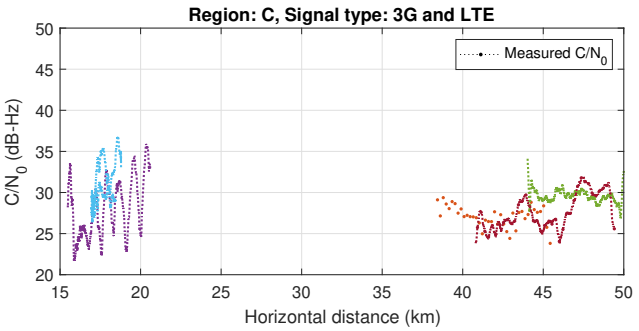

Figure 7. The C/N_0 as a function of the horizontal distance for four 3G towers (blue, red, yellow, and purple) and two LTE towers (green and light blue). The aircraft was flying at an altitude a little above 16,000 ft AGL.

$$\Delta D \triangleq \sqrt{(h_{\rm A}+h_{\rm S})^2+d^2} - \sqrt{(h_{\rm A}-h_{\rm S})^2+d^2},$$
$$\Delta\phi \triangleq \frac{2\pi\Delta D}{\lambda},$$
$$\Gamma(\psi) \triangleq \frac{\epsilon_g \sin\psi - \sqrt{\epsilon_g - \cos^2\psi}}{\epsilon_g \sin\psi + \sqrt{\epsilon_g - \cos^2\psi}},$$

where ϵ_g is the relative permittivity of the ground; $h_{\rm A}$ and $h_{\rm S}$ are the aircraft's and cellular tower's altitude, respectively; d is the horizontal distance; D is the line-of-sight distance; r_p is the antenna radiation pattern defined as $r_p = \cos(\theta)^\beta$, with θ and $\beta = 100$ being the elevation angle and the radiation pattern exponent, respectively; and ψ is the angle between the ground and the reflected ray. The C/N_0 of one 4G towers and one 3G tower as a function of horizontal distance in Region A is shown in Figure 9. For the 4G tower, the far-field two-ray model (green curve) appears to capture the measured C/N_0 (red dots) sufficiently accurately. It is worth noting that the far-field model does not account for the antenna's radiation pattern. However, this did not affect the model fitting, since the tower was already far enough (it was tracked from about 16 km through about 36 km). For the 3G tower, the far-field model (orange curve) did not fit the measured C/N_0 (blue dots) well for small horizontal distances. This discrepancy is due to not accounting for the tower's antenna directivity, which plays a significant role at lower horizontal distances. By accounting to the radiation pattern into the far-field model, a closer fit to the measured C/N_0 was achieved (magenta curve). Nevertheless, a slight mismatch can be seen at horizontal distances less than 10 km, even after accounting for the elevation angle between the aircraft and the cellular tower antenna, which could be due to the fact that the tilting angle of the tower's antenna is not exactly known.

Discussion

The obtained C/N_0 results demonstrate the promise of utilizing cellular signals for aircraft navigation. It was observed that both 3G CDMA and 4G LTE signals exhibited measured C/N_0 between 25 and 55 dB-Hz at altitudes of 2,000–23,000 ft AGL. The aircraft-mounted SDRs were able to maintain reliable tracking of acquired cellular signals throughout as the aircraft ascended/descended along the teardrop flight trajectory. In addition, cellular signals were tracked up to a horizontal distance of 50 km, while flying at about 16,000 ft AGL. These unprecedented results are the first of their kind, showing the tremendous potential of cellular signals for aircraft navigation.

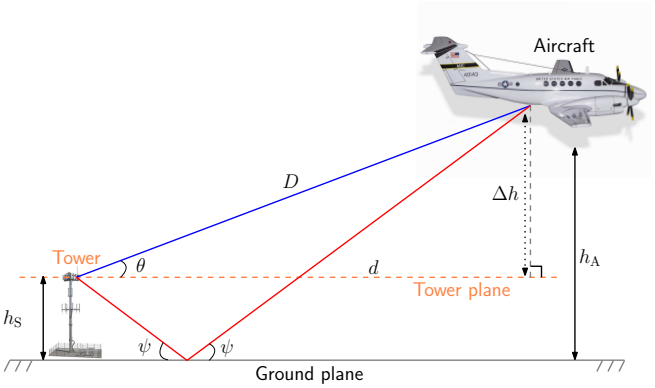

Figure 8. The two-ray model diagram.

The two-ray propagation model appears to fit the measured C/N_0 when flying at an altitude of 16,000 ft AGL, when the cellular transmitter's horizontal distances ranged between 10 km and about 33 km. For distances lower than 10 km, the mismatch between the measured C/N_0 and the two-ray model fit grew. Incorporating the transmitter's antenna radiation pattern reduced this mismatch, albeit did not remove completely. This could be due to the fact that the exact radiation pattern of the transmitter is not precisely known.

4. Conclusion

This paper characterized the received C/N_0 of terrestrial cellular 3G and 4G signals on a Beechcraft C-12 Huron, a fixed-wing U.S. Air Force aircraft. Two types of flight patterns were performed in two different regions. It was observed that cellular signals are surprisingly powerful at both (i) high altitudes, exhibiting C/N_0 of 25–55 dB-Hz at altitudes of 2,000–23,000 ft above ground level (AGL) and (ii) faraway horizontal distances, exhibiting C/N_0 of about 30 dB-Hz for towers as far as 50 km, while flying at about 16,000 ft AGL. In addition, two propagation models were evaluated to describe the behavior of the measured C/N_0: (i) free-space path loss model and (ii) two-ray model. It was observed that the two-ray model fits the measured C/N_0 sufficiently well, for towers more than 10 km away, while flying at an altitude of 16,000 ft AGL. For towers closer than 10 km, the antenna radiation pattern should be incorporated into the two-ray model to improve model fitting.

Acknowledgements

his work was supported in part by the Office of Naval Research (ONR) under Grant N00014-19-1-2511 and Grant N00014-19-1-2613, in part by Sandia National Laboratories under Award 1655264, and in part by the U.S. Department of Transportation (USDOT) under Grant 69A3552047138 for the CARMEN University Transportation Center (UTC). The authors would like to thank Edwards AFB and Holloman AFB for inviting the ASPIN Laboratory to conduct experiments on Air Force aircraft in the "SNIFFER: Signals of opportunity for Navigation In Frequency-Forbidden EnviRonments" flight campaign. The authors would like to thank Joshua Morales, Kimia Shamaei, Mahdi Maaref, Kyle Semelka, MyLinh Nguyen, and Trier Mortlock for their help with preparing for data collection. DISTRIBUTION STATEMENT A. Approved for public release; Distribution is unlimited. 412TW-PA-20146.

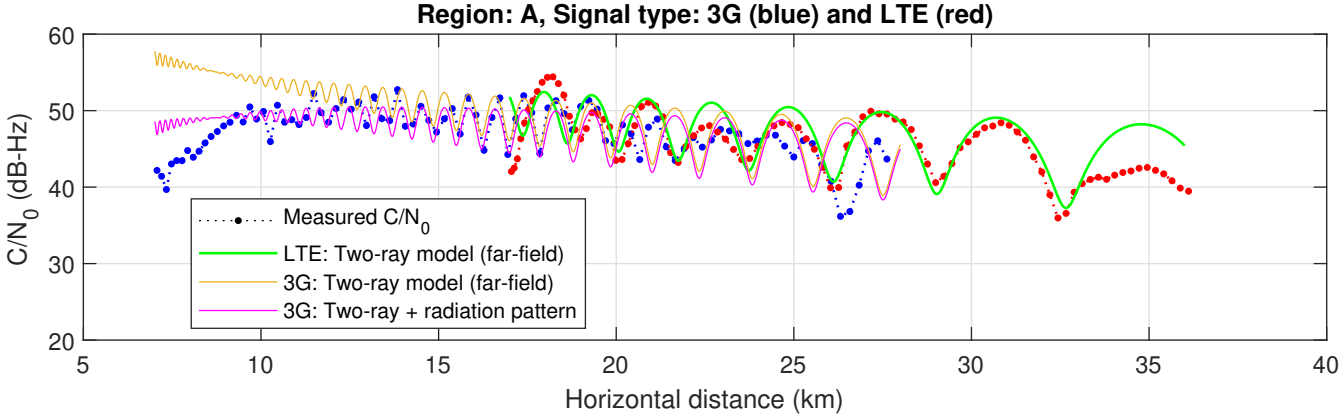

Figure 9. The measured C/N_0 of a 4G tower (red dots) and a 3G tower (blue dots) as a function of horizontal distance in Region A. The model fit is obtained by fitting the measured C/N_0 using the two-ray model and two-ray + cellular tower antenna radiation pattern.

REFERENCES

[1] R. Sabatini, A. Roy, E. Blasch, K. Kramer, , G. Fasano, I. Majid, O. Crespillo, D. Brown, and R. Ogan, "Avionics systems panel research and innovation perspectives," *IEEE Aerospace and Electronic Systems Magazine*, vol. 35, no. 12, pp. 58–72, December 2020.

[2] R. Ioannides, T. Pany, and G. Gibbons, "Known vulnerabilities of global navigation satellite systems, status, and potential mitigation techniques," *Proceedings of the IEEE*, vol. 104, no. 6, pp. 1174–1194, February 2016.

[3] E. Blasch, R. Sabatini, A. Roy, K. Kramer, G. Andrew, G. Schmidt, C. Insaurralde, and G. Fasano, "Cyber awareness trends in avionics," in *Proceedings of IEEE/AIAA Digital Avionics Systems Conference*, 2019, pp. 1–8.

[4] K. Kwon, Y. Jang, C. Yang, and D. Shim, "Impacts of GPS pseudolite signals on GPS software receivers," *Journal of Advanced Navigation Technology*, vol. 16, no. 4, pp. 627–634, August 2012.

[5] T. Marathe, S. Daneshmand, and G. Lachapelle, "Pseudolite interference mitigation and signal enhancements using an antenna array," in *Proceedings of International Conference on Indoor Positioning and Indoor Navigation*, October 2015, pp. 1–9.

[6] J. Grabowski, "Personal privacy jammers: locating Jersey PPDs jamming GBAS safety-of-life signals," *GPS World Magazine*, pp. 28–37, April 2012.

[7] D. Borio, F. Dovis, H. Kuusniemi, and L. Presti, "Impact and detection of GNSS jammers on consumer grade satellite navigation receivers," *Proceedings of the IEEE*, vol. 104, no. 6, pp. 1233–1245, February 2016.

[8] R. La Valle, J. Garcia, and P. Roncagliolo, "Antenna coupling and out of band interference effects on a high precision GNSS receiver," in *Proceedings of Argentine Conference on Electronics*, 2019, pp. 47–51.

[9] C. Hegarty, D. Bobyn, J. Grabowski, and A. Van Dierendonck, "An overview of the effects of out-of-band interference on GNSS receivers," *NAVIGATION, Journal of the Institute of Navigation*, vol. 67, no. 1, pp. 143–161, March 2020.

[10] EUROCONTROL, Aviation Intelligence Unit, "Does radio frequency interference to satellite navigation pose an increasing threat to network efficiency, cost-effectiveness and ultimately safety?" Tech. Rep.

[11] International Civil Aviation Organization (ICAO), "An urgent need to address harmful interferences to GNSS," https://www.iata.org/contentassets/e45e5219cc8c4277a0e80562590793da/address-harmful-interferences-gnss.pdf, Tech. Rep., May 2019.

[12] J. del Peral-Rosado, R. Estatuet-Castillo, J. Lopez-Salcedo, G. Seco-Granados, Z. Chaloupka, L. Ries, and J. Garcoa-Molina, "Evaluation of hybrid positioning scenarios for autonomous vehicle applications," in *Proceedings of ION International Technical Meeting Conference*, January 2017, pp. 2541–2553.

[13] J. del Peral-Rosado, R. Raulefs, J. López-Salcedo, and G. Seco-Granados, "Survey of cellular mobile radio localization methods: From 1G to 5G," *IEEE Communications Surveys Tutorials*, vol. 20, no. 2, pp. 1124–1148, 2018.

[14] T. Kang, H. Lee, and J. Seo, "TOA-based ranging method using CRS in LTE signals," *Journal of Advanced Navigation Technology*, vol. 23, no. 5, pp. 437–443, October 2019.

[15] J. Khalife and Z. Kassas, "Opportunistic UAV navigation with carrier phase measurements from asynchronous cellular signals," *IEEE Transactions on Aerospace and Electronic Systems*, vol. 56, no. 4, pp. 3285–3301, August 2020.

[16] N. Ikhtiari, "Navigation in GNSS denied environments using software defined radios and LTE signals of opportunities," Master's thesis, University of Canterbury, Christchurch, New Zealand, 2019.

[17] P. Wang and Y. Morton, "Multipath estimating delay lock loop for LTE signal TOA estimation in indoor and urban environments," *IEEE Transactions on Wireless Communications*, vol. 19, no. 8, pp. 5518–5530, 2020.

[18] J. Gante, L. Sousa, and G. Falcao, "Dethroning GPS: Low-power accurate 5G positioning systems using machine learning," *IEEE Journal on Emerging and Selected Topics in Circuits and Systems*, vol. 10, no. 2, pp. 240–252, June 2020.

[19] H. Dun, C. Tiberius, and G. Janssen, "Positioning in a multipath channel using OFDM signals with car-

rier phase tracking," *IEEE Access*, vol. 8, pp. 13 011–13 028, 2020.

[20] P. Wang and Y. Morton, "Performance comparison of time-of-arrival estimation techniques for LTE signals in realistic multipath propagation channels," *NAVIGATION, Journal of the Institute of Navigation*, vol. 67, no. 4, pp. 691–712, December 2020.

[21] J. Mortier, G. Pages, and J. Vila-Valls, "Robust TOA-based UAS navigation under model mismatch in GNSS-denied harsh environments," *Remote Sensing*, vol. 12, no. 18, pp. 2928–2947, September 2020.

[22] T. Kazaz, G. Janssen, J. Romme, and A. Van der Veen, "Delay estimation for ranging and localization using multiband channel state information," *IEEE Transactions on Wireless Communications*, pp. 1–16, September 2021.

[23] A. Abdallah and Z. Kassas, "UAV navigation with 5G carrier phase measurements," in *Proceedings of ION GNSS Conference*, September 2021, pp. 3294–3306.

[24] Z. Kassas, "Position, navigation, and timing technologies in the 21st century," J. Morton, F. van Diggelen, J. Spilker, Jr., and B. Parkinson, Eds. Wiley-IEEE, 2021, vol. 2, ch. 38: Navigation with Cellular Signals of Opportunity, pp. 1171–1223.

[25] Z. Kassas, M. Maaref, J. Morales, J. Khalife, and K. Shamaei, "Robust vehicular localization and map matching in urban environments through IMU, GNSS, and cellular signals," *IEEE Intelligent Transportation Systems Magazine*, vol. 12, no. 3, pp. 36–52, June 2020.

[26] M. Driusso, C. Marshall, M. Sabathy, F. Knutti, H. Mathis, and F. Babich, "Vehicular position tracking using LTE signals," *IEEE Transactions on Vehicular Technology*, vol. 66, no. 4, pp. 3376–3391, April 2017.

[27] J. del Peral-Rosado, O. Renaudin, C. Gentner, R. Raulefs, E. Dominguez-Tijero, A. Fernandez-Cabezas, F. Blazquez-Luengo, G. Cueto-Felgueroso, A. Chassaigne, D. Bartlett, F. Grec, L. Ries, R. Prieto-Cerdeira, J. Lopez-Salcedo, and G. Seco-Granados, "Physical-layer abstraction for hybrid GNSS and 5G positioning evaluations," in *Proceedings of IEEE Vehicular Technology Conference*, September 2019, pp. 1–6.

[28] C. Yang and A. Soloviev, "Mobile positioning with signals of opportunity in urban and urban canyon environments," in *Proceedings of IEEE/ION Position, Location, and Navigation Symposium*, April 2020, pp. 1043–1059.

[29] M. Maaref and Z. Kassas, "Autonomous integrity monitoring for vehicular navigation with cellular signals of opportunity and an IMU," *IEEE Transactions on Intelligent Transportation Systems*, 2021, accepted.

[30] J. Khalife and Z. Kassas, "Precise UAV navigation with cellular carrier phase measurements," in *Proceedings of IEEE/ION Position, Location, and Navigation Symposium*, April 2018, pp. 978–989.

[31] K. Shamaei and Z. Kassas, "Sub-meter accurate UAV navigation and cycle slip detection with LTE carrier phase," in *Proceedings of ION GNSS Conference*, September 2019, pp. 2469–2479.

[32] Z. Kassas, J. Khalife, A. Abdallah, and C. Lee, "I am not afraid of the jammer: navigating with signals of opportunity in GPS-denied environments," in *Proceedings of ION GNSS Conference*, 2020, pp. 1566–1585.

[33] G. Athanasiadou, M. Batistatos, D. Zarbouti, and G. Tsoulos, "LTE ground-to-air field measurements in the context of flying relays," *IEEE Wireless Communications*, vol. 26, no. 1, pp. 12–17, February 2019.

[34] X. Cai, N. Wang, J. Rodriguez-Pineiro, X. Yin, A. Yuste, W. Fan, G. Zhang, G. Pedersen, and L. Tian, "Low altitude air-to-ground channel characterization in LTE network," in *Proceedings of European Conference on Antennas and Propagation*, April 2019, pp. 1–5.

[35] W. Khawaja, I. Guvenc, D. Matolak, U. Fiebig, and N. Schneckenburger, "A survey of air-to-ground propagation channel modeling for unmanned aerial vehicles," *IEEE Communications Surveys & Tutorials*, vol. 21, no. 3, pp. 2361–2391, 2019.

[36] A. Abdalla and V. Marojevic, "Communications standards for unmanned aircraft systems: The 3GPP perspective and research drivers," *IEEE Communications Standards Magazine*, vol. 5, no. 1, pp. 70–77, March 2021.

[37] R. Amorim, J. Wigard, I. Kovacs, and T. Sorensen, "UAV communications for 5G and beyond," Y. Zeng, I. Guvenc, R. Zhang, G. Geraci, and D. Matolak, Eds. Wiley-IEEE, 2021, ch. 5: Performance Enhancements for LTE-Connected UAVs: Experiments and Simulations, pp. 139–161.

[38] Qualcomm Technologies, Inc., "LTE unmanned aircraft systems," Tech. Rep. 1.0.1, May 2017. [Online]. Available: https://www.qualcomm.com/documents/lte-unmanned-aircraft-systems-trial-report/

[39] Y. Zeng, Q. Wu, and R. Zhang, "Accessing from the sky: A tutorial on UAV communications for 5G and beyond," *Proceedings of the IEEE*, vol. 107, no. 12, pp. 2327–2375, December 2019.

[40] E. Kim and Y. Shin, "Feasibility analysis of LTE-based UAS navigation in deep urban areas and DSRC augmentation," *Sensors*, vol. 19, no. 9, pp. 4192–4207, April 2019.

[41] P. Misra and P. Enge, *Global Positioning System: Signals, Measurements, and Performance*, 2nd ed. Ganga-Jamuna Press, 2010.

[42] J. Khalife and Z. Kassas, "Navigation with cellular CDMA signals – part II: Performance analysis and experimental results," *IEEE Transactions on Signal Processing*, vol. 66, no. 8, pp. 2204–2218, April 2018.

[43] K. Shamaei and Z. Kassas, "LTE receiver design and multipath analysis for navigation in urban environments," *NAVIGATION, Journal of the Institute of Navigation*, vol. 65, no. 4, pp. 655–675, December 2018.

[44] A. Razavi, D. Gebre-Egziabher, and D. Akos, "Carrier loop architectures for tracking weak GPS signals," *IEEE Transactions on Aerospace and Electronic Systems*, vol. 44, no. 2, pp. 697–710, 2008.

[45] M. Lashley, D. Bevly, and J. Hung, "Performance analysis of vector tracking algorithms for weak GPS signals in high dynamics," *IEEE Journal of Selected Topics in Signal Processing*, vol. 3, no. 4, pp. 661–673, August 2009.

[46] C. Zhu and X. Fan, "A novel method to extend coherent integration for weak GPS signal acquisition," *IEEE Communications Letters*, vol. 19, no. 8, pp. 1343–1346, 2015.

[47] T. Rappaport, *Wireless communications: principles and practice*. Prentice hall PTR New Jersey, 1996, vol. 2.

BIOGRAPHY

Zaher (Zak) M. Kassas *is an associate professor at the University of California, Irvine and director of the Autonomous Systems Perception, Intelligence, and Navigation (ASPIN) Laboratory. He received a B.E. in Electrical Engineering from the Lebanese American University, an M.S. in Electrical and Computer Engineering from The Ohio State University, and an M.S.E. in Aerospace Engineering and a Ph.D. in Electrical and Computer Engineering from The University of Texas at Austin. In 2018, he received the National Science Foundation (NSF) Faculty Early Career Development Program (CAREER) award, and in 2019, he received the Office of Naval Research (ONR) Young Investigator Program (YIP) award. He is a recipient of 2018 IEEE Walter Fried Award, 2018 Institute of Navigation (ION) Samuel Burka Award, and 2019 ION Col. Thomas Thurlow Award. He is an Associate Editor for the IEEE Transactions on Aerospace and Electronic Systems and the IEEE Transactions on Intelligent Transportation Systems. His research interests include cyber-physical systems, estimation theory, navigation systems, autonomous vehicles, and intelligent transportation systems.*

Ali Abdallah *is a Ph.D. student in the Department of Electrical Engineering and Computer Science (EECS) at the University of California, Irvine (UCI) and a member of the Autonomous Systems Perception, Intelligence, and Navigation (ASPIN) Laboratory. He is a recipient of the Best Student Paper Award at the 2020 IEEE/ION Position, Location, and Navigation Symposium (PLANS) and the Grand Prize of the 2020 IEEE Signal Processing Society video contest for beamforming research (5-MICC).*

Joe Khalife *is a postdoctoral fellow at the University of California, Irvine and member of the Autonomous Systems Perception, Intelligence, and Navigation (ASPIN) Laboratory. He received a B.E. in Electrical Engineering, an M.S. in Computer Engineering from the Lebanese American University (LAU) and a Ph.D. in Electrical Engineering and Computer Science from the University of California, Irvine. From 2012 to 2015, he was a research assistant at LAU, and has been a member of the ASPIN Laboratory since 2015. He is a recipient of the 2016 IEEE/ION Position, Location, and Navigation Symposium (PLANS) Best Student Paper Award and the 2018 IEEE Walter Fried Award. His research interests include opportunistic navigation, autonomous vehicles, and software-defined radio.*

Chiawei Lee *is an Assistant Professor and Instructor Flight Test Engineer at the U.S. Air Force Test Pilot School. He serves as the Test Management Program Director where he oversees about a dozen student and staff led flight test projects each year. In addition, he is the Chief Test Safety Officer responsible for the safe execution of curriculum and flight test project safety packages. He received a B.S. in Aerospace Engineering from University of California, Los Angeles and a M.S. in Aero/Astro Engineering from Stanford University.*

Juan Jurado *is a U.S. Air Force Lieutenant Colonel and the Director of Education at the U.S. Air Force Test Pilot School. He holds a B.S. from Texas A&M University, a M.S. from the Air Force Test Pilot School, and M.S. and Ph.D. from the Air Force Institute of Technology. Previously, he served as Director of Engineering for the 413th Flight Test Squadron and oversaw various C-130, V-22, and H-1 flight test programs. His research interests include aircraft performance modeling, online sensor calibration, image processing, visual-inertial navigation, and statistical sensor management for multi-sensor navigation problems.*

Steven Wachtel *is a U.S. Air Force Captian and a Flight Test Engineer, assigned to the 780th Test Squadron, Eglin AFB, FL. He received a B.S. in Mechanical Engineering from The Ohio State University, an M.S. in Flight Test Engineering from the U.S. Air Force Test Pilot School, and an M.S. in Systems Engineering from the Air Force Institute of Technology.*

Thomas Hulsey *is a U.S. Air Force Flight Commander of Operations Engineering. He received a B.S. in Aerospace Engineering from Missouri University of Science and Technology, an M.S. in Aeronautical Engineering from the Air Force Institute of Technology, and an M.S. in Experimental Flight Test Engineering from the United States Air Force Test Pilot School.*

Zachary Hoeffner *is a flight test engineer at the U.S. Air Force. He received a a B.S in Nuclear Engineering from the U.S. Air Force Academy, an M.S. in Flight Test Engineering from the U.S. Air Force Test Pilot School, an M.S. in Engineering Physics and Applied Physics from the Air Force Institute of Technology, and an M.S. in Nuclear Engineering from the Air Force Institute of Technology.*

Jacob Duede *is a Major in the U.S. Air Force. He was trained as a Communication/Navigation/Mission Systems apprentice on C-17 Globmaster II aircraft and stationed at McChord Air Force Base, WA. He graduated from the U.S. Air Force Academy as a commissioned officer with a B.S. in Mechanical Engineering. He attended the Undergraduate Pilot Training at Columbus Air Force Base, MS. In 2020, he graduated from the U.S. Air Force Test Pilot School at Edwards Air Force Base, CA. He is a Senior Pilot with over 2,000 hours and holds an M.S. in Engineering from the University of Arkansas and an M.S. in Flight Test Engineering from Air University.*

Rachel Quirarte *is a KC-46 and KC-135 programmatic flight commander and test pilot in the 418th Flight Test Squadron in the U.S. Air Force. She received a a B.S. in Aeronautical Engineering from the U.S. Air Force Academy, an M.S. in Flight Test Engineering from the U.S. Air Force Test Pilot School, and an M.S. in Mechanical Engineering from Rice University.*

RunXuan Tay *received a B.S. degree in Electrical Engineering from the University California, San Diego and M.S. degree in Flight Test Engineering from the U.S. Air Force Test Pilot School. He is currently a test pilot at Air Warfare Center, Republic of Singapore Air Force, where he works on fixed wing test programs.*